SI-referenced formic acid (HCOOH) spectroscopy at the sub ppt level

Maxime Leuliet, Abdessamad Mbardi, Bérengère Argence, Jean-Philippe Karr, Laurent Hilico

SI-referenced formic acid (HCOOH) spectroscopy at the sub ppt lebel.

Maxime Leuliet[1], Abdessamad Mbardi[1], Bérengère Argence[1], Jean-Philippe Karr[1,2], and Laurent Hilico[1,2]

[1]Laboratoire Kastler Brossel, Sorbonne Université, CNRS, ENS-PSL Research University, Collège de France, 4 place Jussieu, F-75005 Paris, France
[2]Université d'Evry-Val d'Essonne, Université Paris-Saclay, Boulevard François Mitterrand, F-91000 Evry, France

October 11, 2023

Abstract

We report on a new determination of the ν_6, $J' = 21, K'_a = 2, K'_c = 20 \rightarrow J'' = 21, K''_a = 3, K''_c = 19$ HCOOH rovibrational line at 9.17 μm with 40-fold improvement with respect to previous measurements. using a spectrometer referenced to the *Système international* through a frequency comb. The spectrometer has a relative resolution better than 10^{-12}, which together with line shape simulations allows for detailed studies of the modulation, pressure and power shifts and broadenings.

1 Introduction

Optical fiber telecommunication networks enable *Système International* (SI)-referenced ultra stable optical signals around 1.5 μm to be disseminated from national metrology institutes to remote laboratories with stabilities better than 10^{-13} on any time scale and accuracies better than 10^{-14} (cite Refimeve, autre). These features can be transferred to all the teeth of optical frequency combs and hence to any laser which is frequency controlled against the frequency comb, allowing for SI-referenced high resolution spectroscopy [1].

The French REFIMEVE ultrastable signal has recently been delivered at Kastler Brossel laboratory on Jussieu campus in Paris. In this paper, we present the optical frequency synthesis spectrometer we have built for molecular spectroscopy at 9.17 μm and the measurement campaign performed on the ν_6, $J' = 21, K'_a = 2, K'_c = 20 \rightarrow J'' = 21, K''_a = 3, K''_c = 19$ formic acid - HCOOH - rovibrational line.

The experimental setup is described in section 2. It presents the SI-referenced CO_2 laser, the saturated absorption cell, the frequency modulation method and the resulting spectroscopy signal. In section 3, we discuss the lineshape model used to adjust the recorded spectra. The results are presented and discussed in section 4. We obtain a sub ppt (10^{-12}) frequency resolution on the line center and determine pressure and intensity shift coefficients. We show how simulations of the expected line shape including the unresolved hyperfine structure allow understanding the observed linewidth and determining pressure and power broadening coefficients.

2 Experimental setup

2.1 CO_2 laser

Several parts of the experimental setup shown in Fig. 1 have already been described in [4]. The laser source is a single mode CO_2 laser operated on the 9R(42) line with up 800 mW of optical power. The rear mirror of the laser is mounted on a piezo ceramic split in two zones, a short one for fast frequency control and a long one to compensate slow drifts. The beam is split into three parts, one probing the molecular transition, which is frequency shifted by +128 MHz using a double pass acousto-optic modulator (AOM) instead of a single pass AOM in [4], one for frequency control against a 1.5-1.9 μm frequency comb and one to control the frequency of a quantum cascade laser to be used for H_2^+ vibrational spectroscopy.

Figure 1: Experimental setup.

2.2 Saturated absorption cell

HCOOH saturated absorption is performed in a 1.047 m long symmetric Fabry-Perot cavity installed in a vacuum vessel. The mirrors have a 50 m radius of curvature resulting in a beam waist $w_0 = 3.85$ mm. To get stable HCOOH pressure during the measurements, we use a leak valve to inject HCOOH from a small reservoir containing liquid HCOOH and a turbo pump connected to the vacuum vessel through a valve. Both valves are adjusted to get a stable pressure to better than 1% in the vacuum vessel.

The CO_2 laser is injected into the Fabry-Perot cavity with a linear horizontal polarization and mode-matched using a telescope. The empty cavity finesse is 153. We have determined the HCOOH single pass absorption by measuring the cavity maximum transmission using a liquid nitrogen cooled HgCdZnTe detector and a transimpedance amplifier for different HCOOH pressures and found 7.43×10^{-3} μb^{-1} corresponding to an absorption of 7.1×10^{-3} $m^{-1}\mu m^{-1}$. The finesse varies from 143 to 119 when we vary the HCOOH pressure from 0.5 to 2 μb.

The Fabry-Perot cavity is locked on resonance with the CO_2 laser frequency using first harmonic phase sensitive detection on the signal transmitted by the cavity. The modulation frequency is 33 kHz and the modulation depth is ?? kHz. The transmitted signal expressed in volts gives a precise relative scale for the intracavity power or intensity but only an approximate absolute scale of 1.44(14) mW/V for the total power P_o and 0.0618(60) mW/mm^2/V for the intensity on the beam axis I linked by $I = 2P_o/(\pi w_0^2)$. The data analysis is made using the precise scale and the results are converted in physical units with enlarged uncertainties.

2.3 Laser frequency control and modulation

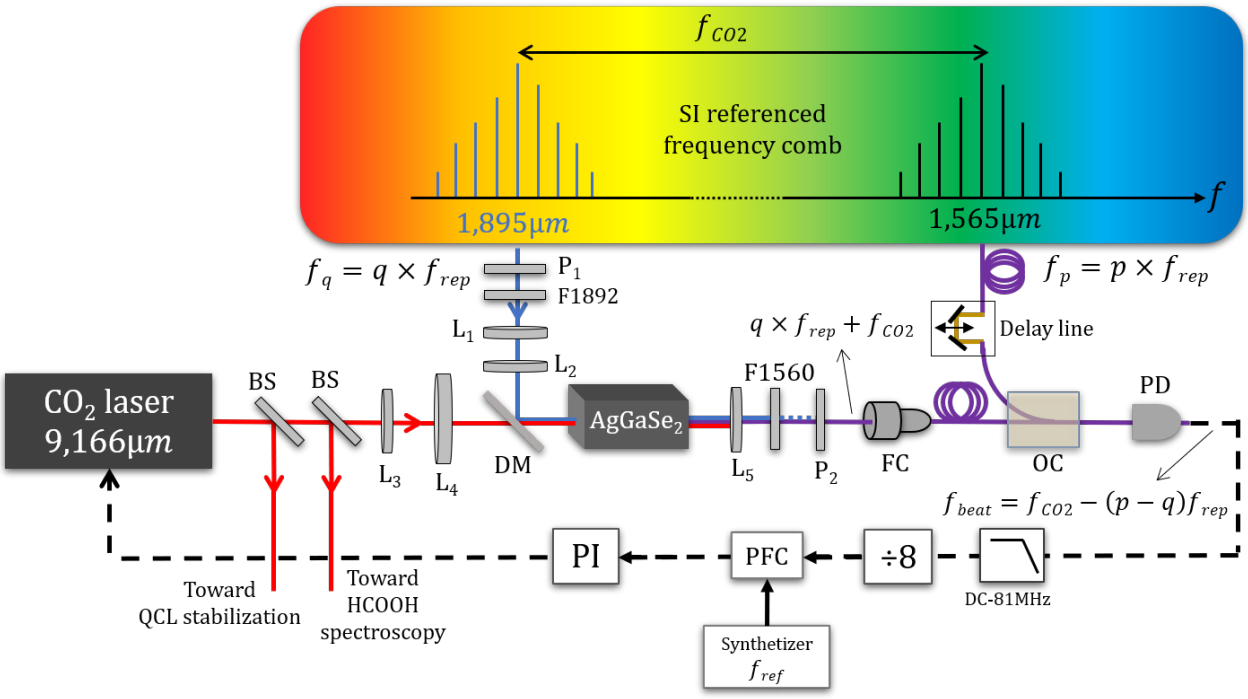

Figure 2: Experimental setup for the stabilization of the CO_2 laser onto the SI refenced frequency comb. The 9.166μm CO_2 beam is overlapped with the 1.895μm part of the frequency comb for sum frequency mixing in a $AgGaSe_2$ crystal. The shifted comb at 1.565μm is combined with the original comb at 1.565μm to produce a beat-note on the photodetector. This beat-note is used to lock the CO_2 laser via a phase lock loop. L_i: Lenses, P_i: Polarizers, DM: dichroic mirror, BS: beam splitter, FC: fiber collimator, OC: optical coupler, PD: photodetector, PFC: phase/frequency comparator.

https://www.overleaf.com/project/6410ec6c615163a4f88ac057

The CO_2 laser frequency is referenced to the *Système Internationnal* (SI) by non-linear mixing

with a near infrared frequency comb [1] as shown in Fig. 2. The comb is carrier offset frequency-free. It is locked optically to the REFIMEVE (cite Refimeve) ultrastable signal with f_{rep} set exactly to 200 MHz. The expected comb teeth frequency stability is better than 10^{-13} at any time scale. The CO_2 laser beam is superimposed and mode matched to the 1.9 μm part of the frequency comb in a 8 mm long $AgGaSe_2$ crystal. With 87 mW of CO_2 laser radiation and 18.4 mW in 56 nm around 1895 nm we generate about 1.1 μW of sum frequency comb radiation at 1.56 nm, corresponding to a conversion efficiency of 0.7 mW/W^2. This radiation is spectrally filtered with a 54 nm wide bandpass filter and is injected in an optical fiber, to be mixed with the original comb in a 75/25% fiber combiner and sent to a fast photodetector for beatnote detection. The pulses are overlapped in time domain using a fibre delay line. The original and shifted comb frequencies have the form $\nu_p = pf_{rep}$ and $\nu_q = qf_{rep}+\nu_{CO_2}$. The beat signal contains peaks at $f_{beat} = \nu_{CO_2}-(p-q)f_{rep}$. The lowest positive beat frequency is close to 64 MHz and is obtained for $p-q = 163\,541$. This beat has a signal to noise ratio up to 53 dB in a 100 kHz bandwidth. It is bandpass filtered, divided by 8 and compared to a reference frequency f_{ref} from a synthesizer using a phase/frequency comparator to obtain a phase error signal. The CO_2 laser servo loop includes a proportional-integral path to the short piezo part, with a loop oscillation frequency of 9 kHz. A second pure integrator slowly acts on the long piezo zone to maintain the fast piezo correction within its working range.

The HCOOH saturated absorption signal is detected using a third harmonic phase sensitive detection (Stanford research SR810). To that end, the reference frequency f_{ref} given by the synthesizer is frequency modulated with a modulation frequency $f_m = 700$ Hz. This modulation is transferred to the CO_2 laser frequency by the feedback loop. The division by 8 and the feedback loop gain at 700 Hz result in an actual modulation depth of $\delta\nu_m = 8.86\ \delta\nu_m$ ranging from 17.72 to 35.44 kHz.

2.4 Measurement strategy

We have systematically recorded spectra for four different HCOOH pressures, four different laser intensities and three different modulation depths with five scans up and five scans down totaling 480 scans. Each scan is made of 178 steps with 160 small 2.5 kHz frequency steps near the center of the line and 9 larger steps to probe the wings on both sides and detect an offset if any. The third harmonic phase sensitive detection time constant is set to 30 ms with a -12 dB/octave roll-off and the dwell time between two measurements is set to 300 ms, larger than the PSD settling time of 210 ms. The noise equivalent bandwidth is 4.2 Hz (from SR810 user's manual). Right before and right after each scan, the HCOOH pressure and transmitted power are measured. These values are used whenever necessary in the spectrum adjustment procedure.

3 Lineshape model

symbol	meaning
f_{rep}	frequency comb repetition rate
ν_{CO_2}	CO_2 laser frequency
f_{beat}	beat-note frequency
ν	laser frequency
ν_c	individual central frequency
$\Delta\nu_{tr}^{th}$	theoretical transit width
$\Delta\nu$	individual line width
x	normalized centered frequency
m	normalized modulation depth
$\delta\nu_m$	laser frequency modulation depth
$\Delta\nu_{FP}$	Fabry-Perot linewidth
S_n	Arndt functions
S_{fit}	S1 + S3 fit function
α_0	vertical offset
$\alpha_{1,3}$	weights
P	HCOOH Pressure
I	Laser intensity
α	pressure broadening coeff
β	coeff for the pressure dependance of the saturation intensity
I_S	saturation intensity

The spectroscopy we perform is in the so called wavelength modulation regime with modulation and demodulation frequencies of 700 and 2100 Hz, much smaller than the limit fixed by the transit time of the molecules in the laser beam profile characterized by a Lorentzian profile with a half width at half maximum (HWHM) given by [5]

$$\Delta\nu_{tr}^{th} = \frac{\sqrt{2ln(2)}}{2\pi w_0}\sqrt{\frac{2k_BT}{m}} = 15.8(10) \text{ kHz}, \tag{1}$$

if probed by a non modulated laser $T = 300$ K. The third derivative of a Lorentzian profile we can expect is perturbed by three effects.

The first one is line shape distortion due to frequency modulation described by Arndt [2] leading to the line shape

$$S_n(x,m) = \frac{i^n\epsilon_n}{2\ m^n}\frac{(\sqrt{(1-ix)^2+m^2}-(1-ix))^n}{\sqrt{(1-ix)^2+m^2}} + c.c., \tag{2}$$

where $x = (\nu - \nu_c)/\Delta\nu$ is the centered normalized laser frequency with ν the laser frequency and $\Delta\nu$ the line HWHM, $m = \delta\nu_m/\Delta\nu$ is the normalized modulation depth and n is the phase sensitive detection order with $\epsilon_0 = 1$ and $\epsilon_{n\geq 1} = 2$.

The second effect is combined frequency-intensity modulation due to the Fabry-Perot cavity. Since the Fabry-Perot is locked on resonance with the laser frequency, the laser frequency modulation at frequency f_m is turned into an intensity modulation at frequency $2f_m$. As a result, contributions of S_1 and S_5 type are added to the S_3 line shape in the case of third harmonic detection. A detailed derivation is given in section 6.

The third effect is line distortion due to unresolved hyperfine structure and is discussed in section 4.3.

The line shape we use for fitting the 480 recorded lines is chosen to be

$$S_{fit}(x,m) = \alpha_0 + \alpha_1 S_1(x,m) + \alpha_3 S_3(x,m) \tag{3}$$

with $x = (\nu - \nu_c)/\Delta\nu$, $m = \delta\nu_m/\Delta\nu$. α_0 is introduced to represent a possible vertical offset, α_1 and α_3 are the weights of the S_1 and S_3 contributions. Note that the S_5 contribution has not been introduced because it is always at least 15 times smaller than the S_1 contribution for $0 \leq m \leq 1.3$, which does not allow accurate determination of S_5 weight and significantly degrades the determination of the other parameters. Fig. 3 shows four typical spectra, their fits with pure S_3 and S_{fit} profiles. One can see that the residuals for S_{fit} are much smaller than those for S_3. For each line, we evaluate the signal to noise ratio (in a 4.2 Hz equivalent bandwidth) as the ratio of the maximum of the signal to the rms of the signal in the wings. It varies from 30 for high pressure, high laser power and low modulation depth up to 160 at low pressure, low intensity and large modulation depth.

4 Results and discussion

For each scan of the formic acid studied here (ν_6 vibrational band, (J' = 21, Ka' = 2, Kc' = 20) $\rightarrow$ (J" = 21, Ka" = 3, Kc" = 19)), individual zero-compatible offsets α_0, weights α_1 and α_3, line centers ν_c, line widths $\Delta\nu$ and error bars are obtained. We do not observe any systematic difference when comparing frequency scan up and frequency scan down. The absence of drag effect is due to the choice of a sufficiently long dwell time. ν_c and $\Delta\nu$ are displayed in Fig 4 and Fig. 5. These quite unusual figures are split in three main columns (one for each modulation depth), which are in turn split in four columns (one for each HCOOH pressure), and finally split into four columns for each laser power. At this latter stage, in Fig. 4, the horizontal axis is used to display the individual values of ν_c whereas in Fig. 5 the horizontal scale locally represents the laser power. The interest of this representation is to also show the pressure and modulation depth trends.

4.1 Central frequency analysis

Figure 4 represents the central frequencies obtained for each of the 480 scans of the rovibrational line of formic acid for the different modulation depths, formic acid pressures P and intracavity intensities I. The data are adjusted by a multilinear fit of the form

$$\nu_c = \nu_0 + AP + BI + C\delta\nu_m \tag{4}$$

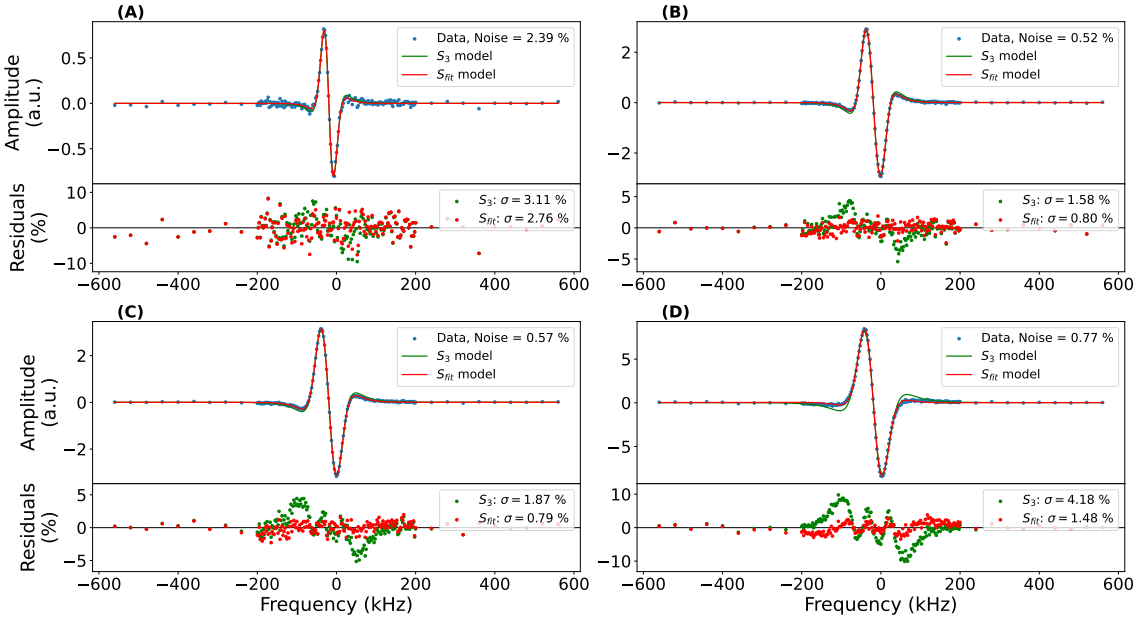

Figure 3: Examples of saturated absorption spectra detected in third harmonic. Experimental parameters (modulation depth, pressure, power) are A: (17720 Hz, 0.5 μb, 0.5 V), B: (35440 Hz, 0.5 μb, 0.5 V), C: (35440 Hz, 1.0 μb, 0.5 V) and D: (35440 Hz, 1.0 μb, 2.0 V). The noise level, estimated from the standard deviation in the wings of the spectra, is given as a percentage of the maximum signal. These profiles are fitted by a simple S_3 model (green) and a S_{fit} model (red). Corresponding residuals are represented at the bottom. The standard deviation σ is comparable to the noise for A configuration having the smallest signal to noise ratio, and is 1.5 to 2 times larger in B, C and D configurations. Horizontal axis: Frequency $= \nu - \nu_{off}$ with $\nu_{off} =$ 32 708 392 000 kHz.

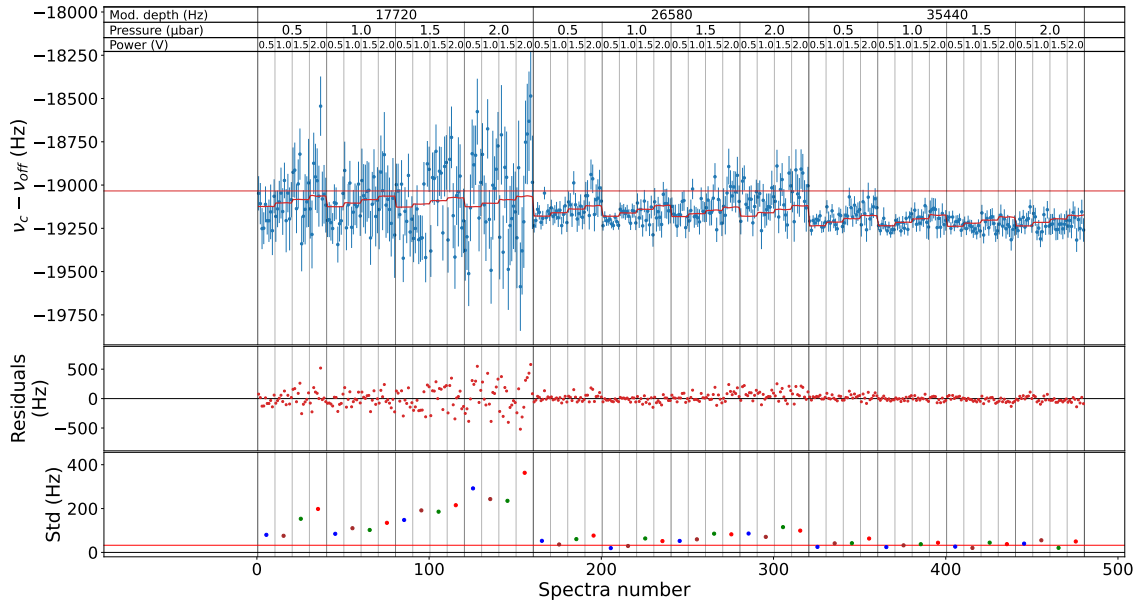

Figure 4: Central frequencies ν_c - ν_{off} obtained from saturated absorption spectra fitted by the S_{fit} model, plotted as a function of modulation depth, formic acid pressure in the Fabry-Perot cavity and intracavity light power. The thick red curve represents a multilinear fit of ν_c by eq. 4 and the horizontal red line shows the estimated undisturbed central frequency ν_0 - ν_{off}. The residuals of the multilinear fit are shown below. The frame at the very bottom of the figure shows the standard deviation of the central frequency over the 10 scans performed for each triplet of parameter values. Points of the same color share a comparable intracavity power. The horizontal red line represents the 10^{-12} level, relatively to the transition frequency.

ν_0 (kHz)	ref.
32 708 391 980.966(18)	this work
32 708 391 981.4(0.8)	[3]
32 708 394(3)	HITRAN

Table 1: ν_6 vibrational band, (J' = 21, Ka' = 2, Kc' = 20) → (J" = 21, Ka" = 3, Kc" = 19) central frequency.

including the measured values of P and I for each scan. In most cases, the residuals are less than the error bars on the central frequencies. *Their standard deviation is equal to 122 Hz, dominated by the contribution at low modulation depth.*

We obtain a pressure line shift A = -0.3(2.8) Hz/μb, which is compatible with 0 and a light shift coefficient B = 41.1(5.7) Hz/V if the intensity is expressed in V, corresponding to B = 666(92) Hz/(mW/mm^2) with an enlarged relative accuracy due to the uncertainty on the transmitted signal to intensity conversion factor. The modulation shift coefficient C = -6.3(0.5) Hz/kHz is significantly different from 0. It comes from a slight asymmetry of the line possibly due to the unresolved hyperfine structure. For the larger modulation depth we used, the correction to the central frequency amounts to +223 Hz. The undisturbed central frequency obtained from the fit is ν_0 = 32 708 391 980 966(18) Hz with a 18 Hz statistical uncertainty (5.5×10^{-13}). This represents a 40 fold improvement with respect to our previous measurement ν_0 = 32 708 391 981.4(0.8) kHz [3].

4.2 Linewidth analysis

Figure 5 shows the HWHM averaged over the 10 scans registered for each modulation depth, pressure and intensity triplet. They vary from 29 to 71 kHz and the corresponding m parameters between 0.25 and 1.22. It clearly shows that the HWHM depend on both the pressure and the intensity but do not depend on the modulation depth, indicating that the S_{fit} profile does indeed deconvolute the modulation effect. Taking into account pressure broadening and power broadening,

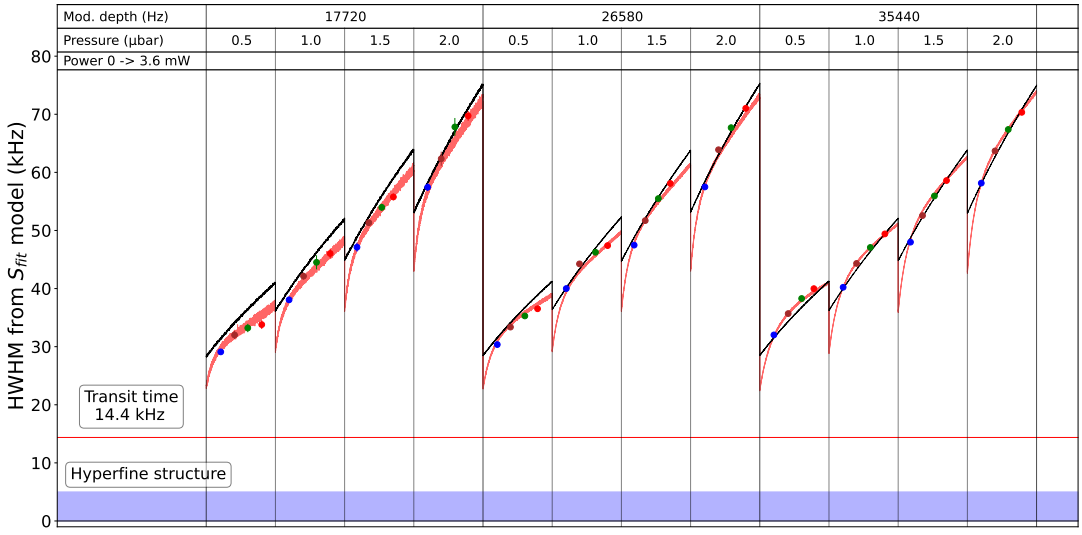

Figure 5: Averaged HWHM obtained by fitting the spectra with S_{fit} model. Dots with the same color share a comparable value of laser intensity. The red and black curves are obtained by fitting simulated spectra as explained in section 4.3. The horizontal red line shows the estimated transit time HMHM of 14.4(1.1) kHz. The blue zone indicates the maximum expected hyperfine splitting, which is not resolved.

the HWHM is expected to vary as

$$\Delta\nu = (\Delta\nu_{tr} + \alpha P)\sqrt{1 + \frac{I}{I_S}} \tag{5}$$

with $\Delta\nu_{tr}$ the transit time HWHM, α the pressure broadening coefficient and I_S the saturation intensity. I_S depends on the linewidth so possibly depends on the pressure. We assume a linear dependence of the form

$$I_S(P) = I_S^0 + \beta P \tag{6}$$

where I_S^0 denote the saturation intensity at zero pressure.

Assuming $\beta = 0$ (we will see later on that the pressure dependence of I_S is small), $\Delta\nu_{tr}$, α and I_S are extracted in the following way: for each $\delta\nu_m$, P and I values, the ten $\Delta\nu^2$ are averaged. A linear fit with the intensity gives twelve determinations of I_S and $\Delta\nu_{tr} + \alpha P$, which are averaged over the three modulation depths. The resulting saturation intensities and zero-intensity widths are plotted against the pressure in Fig. 6 as blue points. This figure shows that the saturation intensity only slightly depends on the pressure, confirming the $\beta = 0$ hypothesis and that the zero-intensity HWHM vary linearly with the pressure. A linear fit gives a preliminary determination of $\Delta\nu_{tr}$ = 20.3(5) kHz . It also give an evaluation of the pressure broadening coefficient α = 16.0(4) kHz/μb as well as the mean saturation power in our cavity, 3.6(0.5) mW, corresponding to a saturation intensity I_S^0=0.154(19) mW/mm^2.

This HWHM analysis is not completely satisfactory for several reasons. First, the transit width does not match the theoretical value. Secondly, the HWHM model of Eq. 5 does not well reproduce the observed HWHM power dependence, as shown by the black lines in Fig. 5. Finally, one can observe in Fig. 5 (B,C and D) that the S_{fit} model has non negligible residuals with reproducible wiggles indicating that the line shape model S_{fit} is not elaborated enough.

4.3 Including the hyperfine structure

Fitting trials have shown that introducing two S_{fit} profiles with different HWHM much improves the residuals with almost no impact on the central frequency determination. Even if unresolved, the hyperfine structure of the lines gives several contributions with close center frequencies and different widths that may explain the observations.

The hyperfine structure of HCOOH has been studied by Chardon [8] and Cazzoli [7] in the case of pure rotational spectroscopy in the ground vibrational level and led to the determination of coupling constants for rotational levels close to those probed in this work. In Section 7, we evaluate the hyperfine structure of the line studied here and show that the line shape can be modeled by the sum of three peaks of the form $S_{th}(x - x_i, m_i)$ given by Eq. 28 and 30 where $x - x_i = (\nu - \nu_i)/\Delta\nu_i$ and $m_i = \delta\nu_m/\Delta\nu_i$ with ν_1 = -4.4 kHz, ν_2 = 0.1 kHz and ν_3 = 4.6 kHz. Direct global fitting of the measured HWHM with this model involving fifteen parameters (a global offset, a central frequency, six amplitudes α_{ki} and the transit time width $\Delta\nu_{tr}$ with three pressure coefficients and three saturation intensities) is not possible due to the unresolved hyperfine structure and too high correlations between the numerous adjustable parameters.

To push further the HWHM analysis, we have decided to address the fitting issue in a different way. The idea is to compute many spectra with an expected profile S_s depending on a reduced number of parameters and to fit the simulated spectra with S_{fit} as for the experimental data in order to reproduce the HWHM behaviour with the pressure and intensity. We have chosen S_s to be given by

$$S_s(x, m) = I_0 \left[S_{th}(x - x_1, m_1) + S_{th}(x - x_2, m_2) + S_{th}(x - x_3, m_1)\right] + \alpha_0. \tag{7}$$

The three terms have the same amplitude. The first and third terms corresponding to the side peaks have the same width $\delta\nu_1$. The second term has the width $\delta\nu_2$. These widths only differ by the associated zero-pressure saturation intensity and are given by

$$\delta\nu_i = (\Delta\nu_{tr} + \alpha P)\sqrt{1 + \frac{I}{I_{S_i}}} \tag{8}$$

where $I_{S_i} = I_{S_i}^0 + \beta P$. S_s thus depends on seven parameters, namely $\Delta\nu_{tr}$, α, β, $I_{S_1}^0$, $I_{S_2}^0$ as well as the zero-pressure cavity HWHM $\Delta\nu_{FP}^0$ and its pressure coefficient η. The two last parameters are determined experimentally (see section 6.3) and are $\Delta\nu_{FP}^0$ = 468 kHz and η = 67.5 kHz/μb.

We simulate spectra for the 48 modulation depth, pressure, intensity triplet values and fit them with S_{fit} to obtain simulated HWHM. These HWHM are in turn fitted to the experimental ones to determine of the five remaining parameters. We obtain $\Delta\nu_{tr} = 14.38(0.15)_{stat}(0.96)_{syst}$ kHz, α = 13.6(0.1) kHz/μb, β = 10.3(4.2)$\times 10^{-4}$ mW/mm^2/μb, $I_{S_1}^0$ = 1.25(0.13)$\times 10^{-2}$ mW/mm^2, $I_{S_2}^0$ = 8.70(0.87)$\times 10^{-2}$ mW/mm^2. The fitting procedure also gives central frequencies, which does not evidence any systematic shift.

Origin	Uncertainty	Uncertainty on central frequency	Uncertainty on $\Delta\nu_{S13}$
pressure	20 nbar	negligible	300 Hz
intracavity power	30 mV	1.2 Hz	$<$ 460 Hz
modulation depth	2%	$<$ 4.5 Hz	$<$ 200 Hz

Table 2: Systematic uncertainties on central frequency and HWHM.

Origin of the width	Frequency
Doppler width	40 MHz
Cavity width	625 kHz
Modulation depth	20-50 kHz
Transit time width	20 kHz
demodulation frequency	2100 Hz
Modulation frequency	700 Hz
Natural width	1 Hz

Table 3: Orders of magnitude of the different frequency width, depth, ...

4.3.1 Comment on $\Delta\nu_{tr}$ and α

The transit time HWHM we obtain, 14.4(1.1) kHz is consistent with the expected value of 15.8(1.0) kHz predicted by Eq. 1 and a new determination of the pressure broadening coefficient $\alpha = 13.6(0.1)$ kHz/μb is obtained. The right part of Fig. 6 clearly show that $\Delta\nu_{tr}$ and α directly obtained from the fit of the experimental data are overestimated and have to be corrected. The dashed line represents the corrected zero-intensity HWHM. The pressure broadening coefficient $\alpha = 13.6(0.1)$ kHz/μb corresponds to 0.460(0.003) cm^{-1}/atm (1 kHz/μb=0.0337983819 cm^{-1}/atm) to be compared with the HITRAN value of 0.32 cm^{-1}/atm.

4.3.2 Comment on saturation intensities and β

The two saturation intensities we obtain differ by a factor 7.8. Saturation intensities are linked to squared dipole matrix element that may vary over orders of magnitude for different hyperfine components [6] making the fitted saturation intensities realistic. The pressure dependence given by $\beta = 10.3(4.2)\times10^{-4}$ mW/mm^2/μb is very small (see the quasi horizontal dashed green lines in the left part of Fig. 6).

4.3.3 Checking the method

To obtain the grey curves in Fig. 6, we have used S_s and the five optimum parameters to simulate spectra for 2000 pressures between 0 and 2.5 μb, the four typical intensities, the three modulation depths and ten realizations of a Gaussian noise with a rms value corresponding to the experimental one. We have applied the same data processing as for the experimental data and obtained the dark grey points. The light grey area corresponds to the error bars.

The red curve in Fig. 5 is obtained in the same way, simulating spectra for 1000 intensities between 0 and 3.6 mW, four pressures, three modulation depths and 10 realizations of Gaussian noise. Only the uncertainty zone is plotted. It shows that the simulated spectra fitted by S_{fit} very well reproduce the experimental HWHM behaviour. The black curve is obtained from a simulation taking into account only one contribution to the width which follows the eq. 5. Disagreement with the experimental data is the basis of this discussion.

5 Conclusion

This simulation of the experimental fitted profiles gives a significant correction to the transit time width towards the expected value, and a significant correction to the pressure broadening from 16.0(0.4) to 13.6(0.1) kHz/μb.

Considering the sources of systematic uncertainty summarized in table 2, we obtain the final results on the absolute central frequency in linear polarization and the broadening due to the transit time:

ν_{abs} = 32 708 391 980 966$(18)_{stat}(6)_{syst}$ Hz.

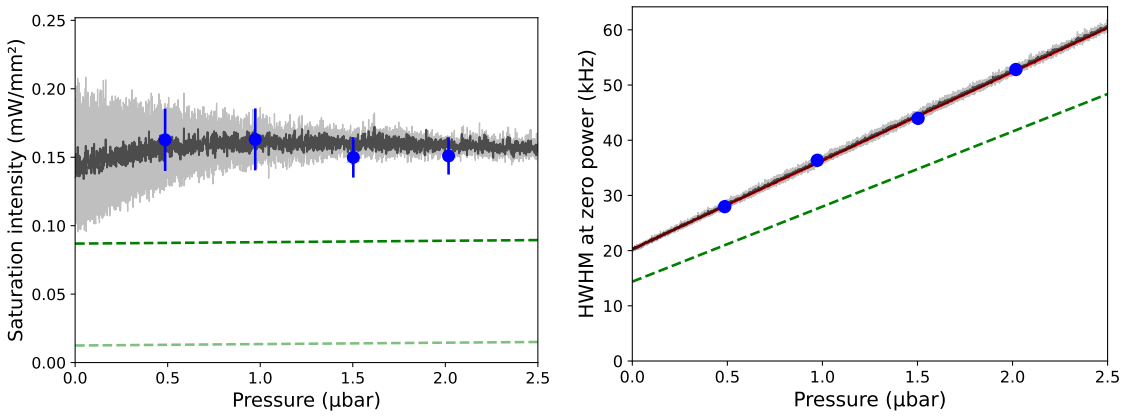

Figure 6: Left: the blue points show the experimental saturation intensity estimated from the model of saturation given by eq. 8 and averaged over the different modulation depths as a function of the formic acid pressure. The nearly horizontal green dashed lines represent the two saturation intensities involved in the simulation model. They show that the pressure dependence is very small. Right: HWHM at zero power extracted with the same method. A linear regression (red line) gives the pressure broadening coefficient and the transit-time HWHM. The green dashed line represents the zero intensity HWHM pressure dependence $\Delta\nu_{tr} + \alpha P$ involved in the simulation model. For both graphs, the blue error bars correspond to the standard deviation of the data for the three modulation depths. The dark grey curve are obtained from simulated spectra using the same algorithm as for experimental data. The light grey area represents the error bars.

6 Appendix: theoretical profile

In this appendix, we first discuss the expected line shape for an isolated transition. To that end, we summarize Arndt derivation of modulation distorted phase sensitive detection signals and extend Schilt derivation of combined intensity modulation (IM) - frequency modulation (FM) to the case of $2f_m$ IM where f_m is the frequency of the modulation frequency. We then discuss the complete line shape model and the simplified models we use.

6.1 Arndt calculation

A Lorentzian line profile is given by

$$t_0(x) = \frac{1}{1+x^2} \tag{9}$$

with $x = \nu/\Delta\nu_{line}$ the reduced laser frequency. When a FM is applied, the instantaneous reduced frequency is

$$x(t) = x_0 + m\cos(2\pi f_m t) \tag{10}$$

and the time dependant spectroscopic signal is the periodic function of time

$$s(t) = t_0(x(t)) = t_0(x_0 + m\cos(2\pi f_m t), \tag{11}$$

that can be expanded in Fourier series as

$$s(t) = \sum_{n=0}^{\infty} S_n(x_0, m)\cos(2\pi\ n f_m t). \tag{12}$$

Phase sensitive detection signals are given by the Fourier coefficients of $s(t)$. Introducing $T_0(y)$ the Fourier transform of $t_0(x)$,

$$T_0(y) = \frac{1}{2\pi}\int_{-\infty}^{\infty} t_0(x)e^{-ixy}dx, \tag{13}$$

Arndt [2] has shown that

$$S_n(x_0, m) = \frac{i^n\epsilon_n}{2\ m^n}\frac{(\sqrt{(1-ix_0)^2+m^2} - (1-ix_0))^n}{\sqrt{(1-ix_0)^2+m^2}} + c.c., \tag{14}$$

with $\epsilon_0 = 1$ and $\epsilon_{n>0} = 2$.

6.2 Fabry-Perot induced IM-FM

For diode laser or quantum cascade laser sources, FM may be obtained using a modulation of the injection current. This method results in combined and phase shifted IM-FM at the same frequency. The effect of IM-FM on line shape has been studied by Schilt in [9].

In this work, we use a CO_2 laser operated very close to the maximum of the emission line. The FM at f_m is applied through the piezo-driven laser cavity length. The spectroscopy signal comes from the transmission of the Fabry Perot cavity, which is locked on resonance with the laser frequency. We have checked that this scheme results in a transmitted (and hence intracavity) IM at frequency $2f_m$ due to the quadratic behaviour of the Fabry-Perot transmission around resonance. No IM at f_m was found. We extend Schilt calculation to this case.

The instantaneous frequency and laser intensity are written

$$\begin{aligned} \nu(t) &= \nu_0 + \delta\nu_m \cos(2\pi f_m t) && (15)\\ I(t) &= I_0\left(1 + qm^2 cos^2(2\pi f_m t - \Psi)\right). && (16) \end{aligned}$$

The IM parameter $q = -4(\Delta\nu/\delta\nu_{FP})^2$ depends on the Fabry-Perot HWHM $\delta\nu_{FP}$. It is introduced in section 6.3. Ψ represents a possible phase shift between IM and FM. Note that Ψ has been introduced in the intensity expression leading to much simpler calculation than in [9].

The spectroscopic signal transmitted by the cavity now reads

$$s(t) = I_0\left(1 + qm^2\cos^2(2\pi f_m t - \Psi)\right)\ t_0(x_0 + m\cos(2\pi f_m t)). \quad (17)$$

The Fourier components of $s(t)$ can be expressed with those of $t_0(x_0 + m\cos(2\pi f_m t))$. Writing

$$s(t) = \sum_{n=0}^{\infty} S_{np}\cos(2\pi n\ f_m t) + S_{nq}\sin(2\pi n\ f_m t), \quad (18)$$

we obtain, for $n \geq 3$

$$\begin{aligned} S_{np} &= \left(1 + \frac{qm^2}{2}\right) S_n(x,m) && (19)\\ &\quad + \frac{qm^2}{4}\cos(2\Psi)(S_{n-2}(x_0,m) + S_{n+2}(x_0,m)),\\ S_{nq} &= \frac{qm^2}{4}\sin(2\Psi)(S_{n-2}(x_0,m) - S_{n+2}(x_0,m)). && (20) \end{aligned}$$

Due to side effects, the formulas for $n = 0$, $n = 1$ and $n = 2$ are different and given by

$$\begin{aligned} S_{0p} &= \left(1 + \frac{qm^2}{2}\right) S_0(x_0,m) + \frac{qm^2}{4} S_2(x_0,m)\cos(2\Psi), && (21)\\ S_{0q} &= 0, && (22)\\ S_{1p} &= \left(1 + \frac{qm^2}{2}\right) S_1(x_0,m), && (23)\\ &\quad + \frac{qm^2}{4}\cos(2\Psi)(S_1(x_0,m) + S_3(x_0,m)),\\ S_{1q} &= \frac{qm^2}{4}\sin(2\Psi)(S_1(x_0,m) - S_3(x_0,m)), && (24)\\ S_{2p} &= \left(1 + \frac{qm^2}{2}\right) S_2(x_0,m), && (25)\\ &\quad + \frac{qm^2}{4}\cos(2\Psi)(2S_0(x_0,m) + S_4(x_0,m)),\\ S_{2q} &= \frac{qm^2}{4}\sin(2\Psi)(2S_0(x_0,m) - S_4(x_0,m)). && (26)\\ & && (27) \end{aligned}$$

Phase sensitive detection with a phase ϕ leads to the profile

$$S_{th}(x,m) = S_{np}(x,m)\cos(\phi) + S_{nq}(x,m)\sin(\phi). \quad (28)$$

In the case of third harmonic detection, the theoretical line shape is

$$S_{th}(x,m) = A_1 S_1(x,m) + A_3 S_3(x,m) + A_5 S_5(x,m), \quad (29)$$

where

$$\begin{cases} A_1 = \dfrac{qm^2}{4}\cos(\phi - 2\Psi) \\ A_3 = \left(1 + \dfrac{qm^2}{2}\right)\cos(\phi) \\ A_5 = \dfrac{qm^2}{4}\cos(\phi + 2\Psi). \end{cases} \tag{30}$$

The coefficients A_1, A_3 and A_5 depend on q, ϕ and Ψ, which are known experimentally. In this work, f_m (700 Hz) is much smaller than the cavity HWHM (600 kHz) so the IM is in phase with the FM such that $\Psi = 0$. ϕ is chosen in order to maximize the detected signal amplitude, and corresponds to $\phi = \pi$ in our case. Moreover, in this configuration, if $\Psi = \pi/4 + k\pi/2$ where k is a relative integer, then the perturbation terms from the first and fifth harmonics vanish. The value of q is discussed in the next paragraph.

6.3 Cavity width and intensity modulation

6.3.1 Pressure dependent cavity width

We consider a Fabry Perot Cavity made of two identical ideal mirrors of reflectivity R and transmission $T = 1 - R$. Absorption by HCOOH in the cavity results in additional losses taken into account by a single pass amplitude transmission factor $\tau = e^{-\xi P/2}$ where P is the pressure. The cavity finesse and maximum transmission are given by

$$F = \pi\sqrt{R\tau}/(1 - R\tau)^2 \tag{31}$$

and

$$T_{max} = (1 - R)^2\tau/(1 - R\tau)^2. \tag{32}$$

They are linked by $F^2 = F_0^2 T_{max}$. The empty cavity finesse F_0 is 153, corresponding to $R = 0.9797$. The empty cavity HWHM is 468 kHz. We have measured the maximum transmission for $P = 0.5$, 1, 1.5 and 2 μb and fitted the results with the above formula, leading to $\xi = 5.92(17) \times 10^{-3}$ μb^{-1}. Varying HCOOH pressure from 0.5 to 2 μb, the single pass transmission τ^2 varies from 99.7 to 98.8%, the maximum transmission from 87.0 to 60.2%, the finesse from 143 to 119. The cavity HWHM given by

$$\Delta\nu_{FP} = \frac{c}{4FL}, \tag{33}$$

varies linearly from 501 to 603 kHz, hence we have $\Delta\nu_{FP} = \Delta\nu_{FP}^0 + \eta P$ with $\Delta\nu_{FP}^0 = 468$ kHz and $\eta = 67.5$ kHz/μb.

6.3.2 Cavity induced intensity modulation

When the cavity is locked on resonance with the laser frequency, the frequency modulation of the laser is turned into intracavity intensity modulation. Both the FM amplitude (at most 35.4 kHz) and the FM frequency ($f_m = 700$ Hz) are much smaller than the cavity width $\Delta\nu_{FP}$. The IM is thus determined by the quadratic behaviour of the intensity build-up close to resonance. Writing the FM $\nu(t) = \nu_0 + \delta\nu_m \cos(2\pi f_m t)$, the intracavity intensity is given by

$$I(t) = I_{max}\left(1 - 4\frac{\delta\nu_m^2}{\Delta\nu_{FP}^2}\cos^2(2\pi f_m t)\right) \tag{34}$$

where I_{max} is the maximum intensity. Introducing the frequency modulation parameter $m = \delta\nu_m/\Delta\nu$, we write $I(t) = I_{max}\left(1 + qm^2\cos^2(2\pi f_m t)\right)$ where the IM parameter q is given by

$$q = -4\left(\frac{\Delta\nu}{\Delta\nu_{FP}}\right)^2. \tag{35}$$

7 HCOOH Hyperfine Structure

To the best of our knowledge, HCOOH hyperfine structure has only be investigated for a limited number of rotational levels in the vibrational ground state of the molecule, first by Chardon [8] and [7]. The spin of the proton attached to the oxygen (resp. carbon) atom are denoted I_1 (resp.

H	M_{aai}	M_{bbi}	M_{cci}
1	-6.904	0.7755	-1.305
2	-6.9275	1.0385	-0.8105

Table 4: M_{ggi} coefficients taken from [7]. Hydrogen 1 is bounded to the oxygen hydrogen 2 is bounded to the carbon atom.

J	K_a	K_c	$\langle J_a^2 \rangle$	$\langle J_b^2 \rangle$	$\langle J_c^2 \rangle$	M_1	M_2
21	2	20	4	387(11)	71(11)	180(9)	317(11)
21	3	19	9	353(10)	100(10)	81(9)	223(11)

Table 5: Extrapolated averaged values of the square of angular momentum components and extrapolated M_1 and M_2 coefficients.

I_2). The coupling scheme is $\mathbf{J}+\mathbf{I_1}=\mathbf{F_1}$ and $\mathbf{F_1}+\mathbf{I_2}=\mathbf{F}$. Hyperfine structure splits each HCOOH rotational level into four sublevels given by

$$E_1 = \frac{M_1+M_2}{2(J+1)} + \frac{\delta}{2(J+1)(2J+3)} \quad (36)$$

$$E_{2,3} = -\frac{M_1+M_2+\delta}{4J(J+1)} \pm \frac{1}{4J(J+1)}\left[(M_1+M_2+\delta)^2 + 4J(J+1)(M_1-M_2)^2\right]^{1/2} \quad (37)$$

$$E_4 = -\frac{M_1+M_2}{2J} + \frac{\delta}{2J(2J-1)}. \quad (38)$$

In these expressions,

- $M_{1,2} = \sum_{g=a,b,c} M_{gg1,2} \langle J_g^2 \rangle$. $M_{gg1,2}$ are the spin rotation constants, the label 1 (resp. 2) corresponding to the hydrogen bounded to the oxygen (resp. carbon) atom. We take the average between the experimental and theoretical values given in [7] (see Table4).
- $\langle J_g^2 \rangle$ are the averaged values of J_g^2 along the principal inertia axis. They are given in [8] for J=2 to 14 and small values of K_a and K_c. One can remark that $\langle J_a^2 \rangle \approx K_a^2$ and that $\langle J_b^2 \rangle$ is quadratic in K_c following the law $\langle J_b^2 \rangle = 0.78(5)K_c^2 + 3.55(43)K_c + 1.12(75)$. Finally, $\langle J_c^2 \rangle$ is given by $J(J+1) - \langle J_a^2 \rangle - \langle J_b^2 \rangle$. Extrapolated values of $\langle J_g^2 \rangle$ and $M_{1,2}$ are given in Table 5.
- δ is the spin-spin interaction matrix element. It depends on J. δ values given in [8] for J from 2 to 14 can be extrapolated with a quadratic law of the form $1.84(7)J^2 - 43(6)$. The extrapolation gives δ = -769(27) kHz for J=21.

The resulting hyperfine splittings are given in Table 6. Figure 7 shows the stick spectrum evaluated using standard angular algebra formula (last equation in [8]). It shows that the main hyperfine components form a narrow quadruplet with peaks located at $\Delta E_1 = -4.4$ kHz, $\Delta E_2 = 0.2$ kHz, $\Delta E_3 = 0.0$ kHz and $\Delta E_4 = 4.6$ kHz from the hyperfine-less transition frequency, with respective weights 1.044, 0.998, 0.998 and 0.951. The position of the peaks mainly depends on M_1 and M_2 values with 0.2 to 0.3 kHz contributions to the uncertainties but only hardly depends on δ with less than 0.02 kHz contributions. The quadratic sum of all contributions is about 0.5 kHz.

These four main hyperfine components span less than 10 kHz (see Fig. 7). This is slightly smaller than the transit time HWHM of the spectrometer. Hyperfine structure is unresolved but may explain the non-zero residuals of S_{fit} we observe.

8 Conclusion

Using a SI-referenced frequency comb allowed to carry out a study of systematic effects of the pressure, the intensity and the modulation depth on the formic acid rovibrational transition central frequency. The absolute central frequency has been determined with a relative statistic uncertainty

J	K_a	K_c	E_1	E_2	E_3	E_4
21	2	20	10.9	3.3	-3.0	-12.3
21	3	19	6.5	3.6	-3.1	-7.7

Table 6: Extrapolated hyperfine structure splittings in kHz.

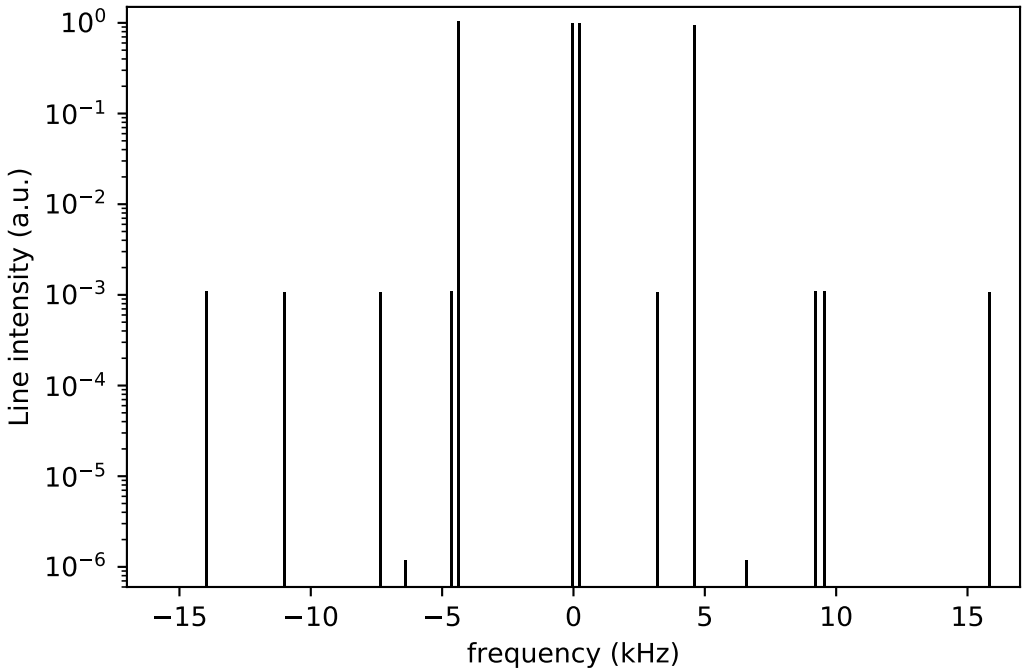

Figure 7: Stick spectrum of the fourteen hyperfine transitions in units of the reduced transition matrix element. Cross over lines are not shown.

model	nb of lines	weights	widths	transit	α	I_{S_1}	I_{S_2}	β
				kHz	kHz/μb	V	V	V/μb
1	3	111	lnl	14.38(15)	13.60(10)	0.202(8)	1.408(18)	0.017(7)
2	3	121	lnl	16.64(25)	14.21(15)	0.218(21)	1.494(39)	0.010(23)
3	3	121		19.68(85)	16.14(64)		2.139(339)	0.124(227)
4	1	1		20.62(86)	16.09(63)		2.212(364)	0.139(240)
5	3	111		19.66(84)	15.95(55)		2.252(364)	0.031(213)
6	2	11	nl	17.28(21)	14.52(13)	0.264(25)	1.802(41)	0.029(24)
7	2	12	nl	14.53(15)	13.49(11)	0.185(8)	1.362(19)	0.019(7)

model	σ_A	σ_B	σ_C	σ_D	quadr. sum
1	2.84	0.97	0.94	0.87	3.26%
2	2.94	0.90	0.89	1.29	3.45%
3	3.41	1.70	1.75	4.52	6.17%
4	3.26	1.58	1.63	4.38	5.91%
5	3.52	1.69	1.78	4.62	6.31%
6	2.97	1.03	1.03	1.76	3.75%
7	2.83	0.94	0.91	0.95	3.26%

Table 7: Different line shape models, transit HWHM, pressure broadening coefficient, saturation intensity(ies), β given with their statistical uncertainties given by the covariance matrix. Column widths: n=narrow, l=large. The models 6 and 7 consider two superposed lines.

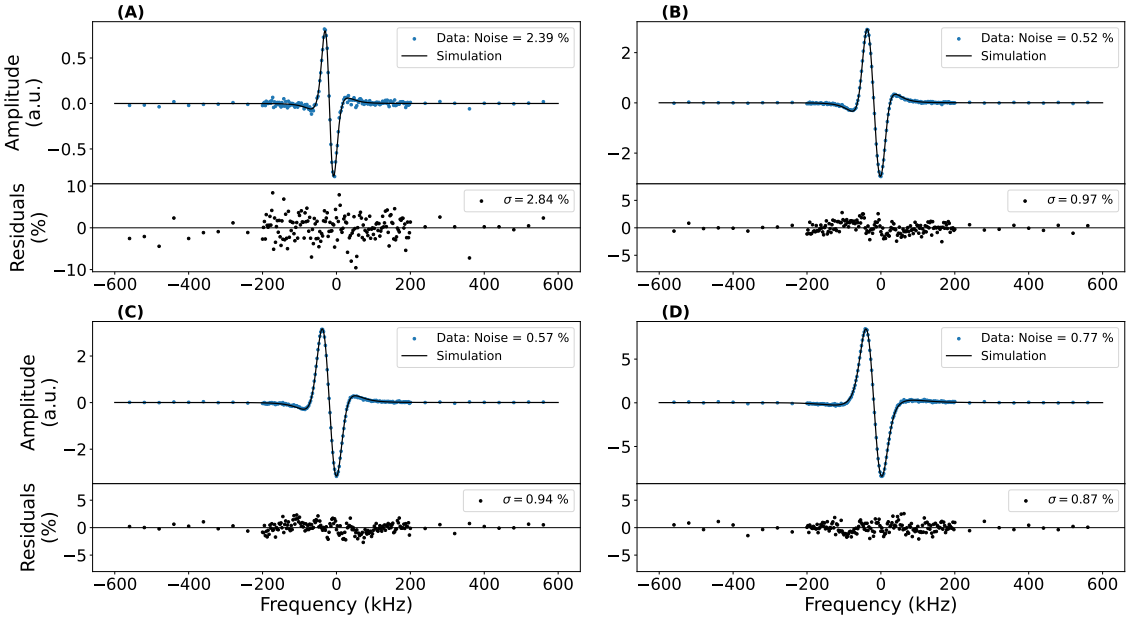

Figure 8: Experimental spectra same as in figure 3 compared to the corresponding generated spectra from the simulation model. The experimental triplets of pressure, power and modulation depth determine the values of m_1 and m_2 in eq. 7. The offset central frequency, global amplitude and vertical offset are adjusted. The simulated spectra are in very good agreement with experimental spectra on the entire range of values of experimental parameters.

less than 10^{-12}, which is the main objective required to the next study on H_2^+ molecule. The residuals obtained from experimental profiles fitted by various models have enabled to develop a theoretical model taking into account of combined effects of the modulation depth, the intensity modulation induced by the frequency modulation and the hyperfine structure on the observed line shapes. This study allowed us to fix bias concerning the determination of optimal parameters involved in the two-width model and then estimate a limit width due to the transit time compatible with its expected value. This model reproduces very well the observed widths and experimental line shapes. The hypothetical origin of distinct widths due to the hyperfine structure may be tested by carrying out a similar study on a molecule which does not have a hyperfine structure. If the line shape distortions are explainable by contributions of different widths, then the hypothesis would be rejected.

Acknowledgement

This work was supported by the LABEX Cluster of Excellence FIRST-TF (ANR-10-LABX-48-01), within the Program « Investissements d'Avenir » operated by the French National Research Agency (ANR). It was also supported by Region Ile de France DIM QUANTIP and DIM SIRTEQ (Coqteil grant), and by ANR-19-CE30-0029 HYMPE grant.

References

[1] Bérengère Argence, Bruno Chanteau, Olivier Lopez, Daniele Nicolodi, Michel Abgrall, Christian Chardonnet, Christophe Daussy, Benoît Darquié, Yann Le Coq, and Anne Amy-Klein. Quantum cascade laser frequency stabilization at the sub-hz level. *Nature Photonics*, 9(7):456–460, jun 2015.

[2] Rolf Arndt. Analytical line shapes for lorentzian signals broadened by modulation. *Journal of Applied Physics*, 36(8):2522–2524, aug 1965.

[3] Franck Bielsa, Khelifa Djerroud, Andrei Goncharov, Albane Douillet, Tristan Valenzuela, Christophe Daussy, Laurent Hilico, and Anne Amy-Klein. Hcooh high-resolution spectroscopy in the 9.18 μm region. *Journal of Molecular Spectroscopy*, 247(1):41 – 46, 2008.

[4] Franck Bielsa, Albane Douillet, Tristan Valenzuela, Jean-Philippe Karr, and Laurent Hilico. Narrow-line phase-locked quantum cascade laser in the 9.2 μm range. *Opt. Lett.*, 32(12):1641–1643, Jun 2007.

[5] C. J. Bordé, J. L. Hall, C. V. Kunasz, and D. G. Hummer. Saturated absorption line shape: Calculation of the transit-time broadening by a perturbation approach. *Physical Review A*, 14(1):236–263, jul 1976.

[6] J. Bordé and Ch.J. Bordé. Intensities of hyperfine components in saturation spectroscopy. *Journal of Molecular Spectroscopy*, 78(3):353–378, 1979.

[7] G. Cazzoli, C. Puzzarini, S. Stopkowicz, and J. Gauss. Hyperfine structure in the rotational spectra of trans-formic acid: Lamb-dip measurements and quantum-chemical calculations. *Astronomy and Astrophysics*, 520:A64, sep 2010.

[8] Jean-Claude Chardon, Claude Genty, Daniel Guichon, and Jean-Gérard Theobald. rf spectrum and hyperfine structure of formic acid. *The Journal of Chemical Physics*, 64(4):1437–1441, feb 1976.

[9] Stéphane Schilt, Luc Thévenaz, and Philippe Robert. Wavelength modulation spectroscopy: Combined frequency and intensity laser modulation. *Applied Optics*, 42(33):6728, 2003.